On modelling the Fast Radio Burst population and event rate predictions

Apurba Bera,[1]⋆ Siddhartha Bhattacharyya,[1]⋆ Somnath Bharadwaj,[1,2]
N. D. Ramesh Bhat[3,4] and Jayaram N. Chengalur[5]

[1]*Department of Physics, Indian Institute of Technology, 721302 Kharagpur, India*
[2]*Centre for Theoretical Studies, Indian Institute of Technology, 721302 Kharagpur, India*
[3]*Australian Research Council Centre of Excellence for All-Sky Astrophysics (CAASTRO) Redfern, NSW 2016, Australia*
[4]*International Centre for Radio Astronomy Research, Curtin University, Bentley, WA 6102, Australia*
[5]*National Centre for Radio Astrophysics, Tata Institute of Fundamental Research, Pune 411007, India*

ABSTRACT

Assuming that Fast Radio Bursts (FRBs) are of extragalactic origin, we have developed a formalism to predict the FRB detection rate and the redshift distribution of the detected events for a telescope with given parameters. We have adopted FRB 110220, for which the emitted pulse energy is estimated to be $E_0 = 5.4 \times 10^{33}$ J, as the reference event. The formalism requires us to assume models for (a) pulse broadening due to scattering in the ionized intergalactic medium – we consider two different models for this, (b) the frequency spectrum of the emitted pulse – we consider a power-law model $E_\nu \propto \nu^{-\alpha}$ with $-5 \leq \alpha \leq 5$, and (c) the comoving number density of the FRB occurrence rate $n(E, w_i, z)$ – we ignore the z dependence and assume a fixed intrinsic pulse width $w_i = 1$ ms for all the FRBs. The distribution of the emitted pulse energy E is modelled through (a) a delta function where all the FRBs have the same energy $E = E_0$, and (b) a Schechter luminosity function where the energies have a spread around E_0. The models are all normalized using the four FRBs detected by Thornton et al. Our model predictions for the Parkes telescope are all consistent with the inferred redshift distribution of the 14 FRBs detected there to date. We also find that scattering places an upper limit on the redshift of the FRBs detectable by a given telescope; for the Parkes telescope, this is $z \sim 2$. Considering the upcoming Ooty Wide Field Array, we predict an FRB detection rate of ~ 0.01 to $\sim 10^3$ d^{-1}.

Key words: cosmology: observations.

1 INTRODUCTION

In the recent past, a new class of radio bursts of millisecond duration, called Fast Radio Bursts (FRBs), have been detected at the Parkes and Arecibo telescopes (Lorimer et al. 2007; Thornton et al. 2013; Spitler et al. 2014). The observed pulses show a dispersion index of -2.000 ± 0.006 and a scattering index of -4.0 ± 0.4 both of which are the signatures of propagation through cold plasma. All of the FRBs barring FRB 010621 have been detected at high Galactic latitudes ($|b| > 5°$) and the large dispersion measure (DM ~ 400–1100 pc cm^{-3}) of these pulses exceed the expected Galactic contribution predicted by the NE2001 model (Cordes & Lazio 2002) in the direction of the bursts by a factor of ~ 10–20 in most of the cases. This indicates an extragalactic origin of the FRB sources. Note that Loeb et al. (2014) have suggested an alternate interpretation where the FRBs may be of Galactic origin; however, we do not

consider this possibility here. The observed flux density together with the redshift inferred from the extragalactic contribution to the DM implies that an enormous amount of energy ($\sim 10^{31}$–10^{33}J) is released in each burst. Further, the source size of ~ 100 km inferred from the pulse widths of ~ 1 ms imply extreme environments in these sources. Unfortunately, no counterpart has yet been detected in any other part of the electromagnetic spectrum, which makes it difficult to determine the physical origin of the FRBs (Petroff et al. 2015).

Several models have been proposed for the source of the FRBs. These include supermassive neutron stars (Falcke & Rezzolla 2014), binary neutron star mergers (Totani 2013), binary white dwarf mergers (Kashiyama et al. 2013), flaring stars (Loeb et al. 2014), pulsar companions (Mottez & Zarka 2014) and many more. However, we are still far from having enough information to validate any of these models.

14 out of the 16 FRBs so far (Table 1) were detected with the Parkes telescope, nine of which were discovered by the High Time Resolution Universe (HTRU) survey. The Parkes radio telescope is a fully steerable single dish telescope of 64 m diameter. The Parkes

⋆E-mail: apurbabera@iitkgp.ac.in (AB); siddhartha@phy.iitkgp.ernet.in (SB)

Table 1. Reported FRBs to date: this list contains a total of 16 events among which FRB 121102 and FRB 110523 were detected at Arecibo and Green Bank Telescope, respectively while the remaining 14 were all detected at Parkes. The FRB parameters, including the redshifts are taken from the published references listed in the table. Champion et al. (2015) have not mentioned the redshift but provide DM_{MW} from which we have estimated z using equation (10). Note that none of the FRBs have a direct redshift measurement, and the z values in this table have all been inferred from the observed DM. Bannister & Madsen (2014) have proposed that FRB 010621* probably has a Galactic origin in which case the estimated redshift is not meaningful. However, in our work we assume an extragalactic origin for this FRB and take the estimated redshift to be correct.

FRB	Peak flux density (Jy)	Pulse width (ms)	FRB Measured Fluence (Jy ms)	DM (pc cm^{-3})	z	Spectral index	Reference
FRB 010621*	0.4	7.8	3.12	746	0.1	–	Keane et al. (2012)
FRB 010724	30	4.6	140	375	0.1	-4 ± 1	Lorimer et al. (2007)
FRB 011025	0.3	9.4	2.8	790	0.6	–	Burke-Spolaor & Bannister (2014)
FRB 090625	0.5	4.4	>2.2	900	0.9	–	Champion et al. (2015)
FRB 110220	1.3	5.6	8.0	944	0.8	–	Thornton et al. (2013)
FRB 110523	0.6	<6.3	3.8	623	0.5	-7.8	Masui et al. (2015)
FRB 110627	0.4	<1.4	0.7	723	0.6	–	Thornton et al. (2013)
FRB 110703	0.5	<4.3	1.8	1104	1.0	–	Thornton et al. (2013)
FRB 120127	0.5	<1.1	0.6	553	0.5	–	Thornton et al. (2013)
FRB 121002	0.4	2.1, 3.7	1.5	1629	1.5	–	Champion et al. (2015)
FRB 121102	0.4	3.0	1.2	557	0.3	7 to 11	Spitler et al. (2014)
FRB 130626	0.5	3.2	>1.5	952	0.9	–	Champion et al. (2015)
FRB 130628	0.9	1.4	>1.2	470	0.4	–	Champion et al. (2015)
FRB 130729	0.1	23.4	>3.5	861	0.8	–	Champion et al. (2015)
FRB 131104	1.1	<0.6	0.6	779	0.6	0.3 ± 0.9	Ravi et al. (2015)
FRB 140514	0.5	2.8	1.3	563	0.4	–	Petroff et al. (2015)

multibeam receiver has 13 independent beams each with a narrow field of view (FoV) of 14.4 arcmin (HPBW). The combination of low system noise (27 K) and a large gain ($G = 0.74$ KJy^{-1}) of the primary beam makes it one of the most sensitive single dish telescopes currently in operation. The HTRU survey uses L-band receivers operating at ∼1.4 GHz with a bandwidth of 400 MHz.

All the FRBs (except FRB 110523), to date (Table 1), have been detected in the L-band (∼1–2 GHz) and their emission spectrum is not constrained, though it appears that they may be consistent with a flat spectrum. Detections with telescopes operating at lower frequencies will place strong constraints on the spectrum which in turn will yield very important constraints on models for the origin of the FRBs. Currently all that is available are constraints on spectral indices and event rates of FRBs from non-detections in observations at lower frequencies (Coenen et al. 2014; Karastergiou et al. 2015).

The Ooty Radio Telescope (ORT[1]) is a parabolic cylindrical reflector of dimensions 530 m × 30 m which operates at a nominal frequency of $\nu_o = 326.5$ MHz with a bandwidth of 4 MHz. It has a linear array of 1056 half-wavelength dipoles placed nearly end to end along the focal line of the cylindrical reflector. Since the dipoles are all oriented along the same direction, the telescope is sensitive to only a single linear polarization component. The ORT currently operates as a single antenna which combines the signal from all the 1056 dipoles. We refer to this as the ORT Legacy system (LS). Work is currently in progress to upgrade the ORT so that it is possible to combine different numbers (N_d) of successive dipoles to form many (N_A) smaller individual antennas which can functions as a linear interferometric array, the Ooty Wide Field Array (OWFA; Prasad & Subrahmnya 2011a,b; Subrahmanya, Manoharan & Chengalur, in preparation). At completion, we expect to have OWFA Phase I (PI), OWFA Phase II (PII) and the LS, all of which can function in parallel, and for which a few relevant parameters are summa-

rized in Table 2. The large FoV and reasonably high sensitivity makes all three versions of the ORT (LS,PI and PII) very promising instruments for detecting FRBs. The PII, in particular, has an FoV that is 880 times larger than that of Parkes while the system noise is only five times larger. While the two instruments work at different frequencies, this comparison gives an idea of the tremendous potential of detecting a large number of FRBs. The two other versions (LS and PI) will probe smaller FoVs with deeper sensitivity. We expect the three versions together provide very interesting and useful inputs as to the FRB population and the origin of the FRBs.

In this paper, we assume the FRBs to be of cosmological origin, and set up a general framework for predicting the detection rate for a telescope with given parameters. As mentioned earlier, very little is known about the FRBs and it is necessary to make several assumptions to make progress. To this end, we introduce a power-law model for the spectral energy density of an FRB and calculate the fluence and pulse width that will be observed accounting for the various propagation effects including dispersion and scattering in the intergalactic medium (IGM). We use this to determine an FRB detection criteria. It is also necessary to specify the comoving number density of the FRB occurrence rate $n(E, w_i, z)$ as a function of the pulse energy E, its intrinsic width w_i, and the redshift z. We have considered two simple models, both of which assume $n(E, w_i, z)$ to be independent of z over the relevant redshift range. The models are all normalized to the FRB detection rate observed at the Parkes telescope. Finally, we use the entire framework to make predictions for the FRB detection rate for the three different versions of the ORT (LS, PI and PII) which, in principle, can work commensally.

A brief outline of the paper follows. The framework for calculating the detection rate is presented in Section 2. Section 3 presents the models for the FRB population, and we present the detection rates predicted for the three versions of ORT in Section 4. The summary and conclusions are presented in Section 5.

---

[1] http://rac.ncra.tifr.res.in/

Table 2. This shows the system parameters for the ORT LS and the upcoming Phase I and Phase II of OWFA. The aperture efficiency (η) is approximately 0.6, the system temperature (T_{sys}) is 150 K for all the three systems and ΔS(1 ms) is the 1σ noise for incoherent addition of the antenna signals with integration time of 1 ms. For reference, the Parkes telescope has a FoV (HPBW) of $0°.23 \times 0°.23$ and $[\Delta S]_{1ms} = 0.05$ Jy in the L-band. We note that it is necessary to do offline beam forming to achieve the angular resolution quoted here for OWFA Phases I and II. For this paper we have only considered incoherent addition where the angular resolution is the same as the FoV listed here.

Parameter	ORT Legacy	OWFA Phase I	OWFA Phase II
Number of dipoles (N_d)	1056	24	4
Number of antennas (N_A)	1	40	264
Aperture dimensions ($b \times d$)	530 m × 30 m	11.5 m × 30 m	1.9 m × 30 m
FoV	$0°.1 \times 1°.75$	$4°.6 \times 1°.75$	$27°.4 \times 1°.75$
Angular resolution	$0°.1 \times 1°.75$	7 arcmin × $1°.75$	6.3 arcmin × $1°.75$
Bandwidth B in MHz	4	18	30
Spectral resolution ($\Delta\nu_c$) in kHz	125	24	48
$[\Delta S]_{1ms}$ in Jy	0.343	1.179	2.151

FRB 110220 detected by Thornton et al. (2013) is the second brightest event observed so far (after the so-called Lorimer burst; Lorimer et al. 2007), and it is the best characterized FRB at present. We have adopted FRB 110220 as the reference event for our entire analysis. FRB 110220 was detected in beam 03 of the Parkes multibeam receiver; however, its exact position relative to the beam centre is not known. For our analysis we have made the conservative assumption that it is located close to the beam centre, i.e. the intrinsic fluence is almost equal to the observed fluence. For our calculations we assume that the Parkes has a Gaussian beam shape.

It is important to note that currently no FRB has an independent redshift measurement, and all the redshifts quoted in Table 1 have been inferred from the measured DM which is assumed to be a sum of three components. The NE2001 model (Cordes & Lazio 2002) gives an estimate of the Milky Way contribution in the direction of the FRB. The contribution from the FRB host galaxy is unknown, and different authors have used different values for this. The residual DM, after accounting for these two components, is attributed to an uniform, completely ionized IGM and this is used to infer the FRB's redshift. Both the Milky Way ISM and the IGM are clumpy and turbulent, and the respective DM contributions along the actual line of sight to the FRB will differ from the model prediction used to infer the redshift. There is further uncertainty in the inferred redshift as there is no estimate for the host contribution. It is possible to avoid this last uncertainty to some extent by setting the host contribution to zero whereby we may interpret the inferred redshift as an upper limit to the actual redshift of the FRB (Keane & Petroff 2015). The various uncertainties in the FRB models adopted later in this paper far outweigh the uncertainties in the inferred redshifts, and for this work we have adopted the values quoted in Table 1.

We have used $(\Omega_m, \Omega_\Lambda, \Omega_b, h) = (0.32, 0.68, 0.04, 0.7)$ for the cosmological parameters (Spergel et al. 2003).

2 BASIC FORMALISM

We assume that the spectral energy density E_ν emitted by an FRB can be expressed as

$$E_\nu = E\phi(\nu) \tag{1}$$

where $\phi(\nu)$ is the emission profile. As mentioned earlier, we have used FRB 110220 as the fiducial event for our analysis. This FRB was inferred to have a redshift $z = 0.8$, for which the Parkes observational frequency band from 1182 to 1582 MHz corresponds to

the frequencies $\nu_a = 2128$ MHz and $\nu_b = 2848$ MHz, respectively in the rest frame of the source.

We have used the frequency interval from $\nu_a = 2128$ MHz to $\nu_b = 2848$ MHz to normalize the emission line profile of all the FRBs such that

$$\int_{\nu_a}^{\nu_b} \phi(\nu)\,d\nu = 1. \tag{2}$$

Here E (equation 1) is the energy emitted by the FRB in the frequency interval ν_a to ν_b, and we henceforth refer to E simply as the 'energy' emitted by the FRB. For reference, the energy emitted by FRB 110220 is estimated to be $E_0 = 5.4 \times 10^{33}$ J which we use as the fiducial value of E throughout this paper.

We now consider observations of an FRB of energy E at redshift z. The number of photons emitted in the frequency interval $d\nu_{src}$ centred around ν_{src} in the rest frame of the source is given by

$$dN_{photon} = \frac{E\phi(\nu_{src})\,d\nu_{src}}{h_p \nu_{src}} \tag{3}$$

where h_p is the Planck constant. The same number of photons will be received in the frequency interval $d\nu_{obs} = (1+z)^{-1}\,d\nu_{src}$ centred around the frequency $\nu_{obs} = (1+z)^{-1}\,\nu_{src}$ at the observer. The fluence $F_{\nu_{obs}}$ observed in this frequency interval is

$$F_{\nu_{obs}} = \frac{dN_{photon} h_p \nu_{obs}}{4\pi r^2 d\nu_{obs}}. \tag{4}$$

where r is the comoving distance corresponding to redshift z. The usual unit of comoving distance is Mpc. Using equations (3) and (4), we have

$$F_{\nu_{obs}} = \frac{E\phi(\nu_{obs}(1+z))}{4\pi r^2}. \tag{5}$$

We now introduce the assumption that the observations are being carried out using a telescope with an observational frequency band from ν_1 to ν_2. In this context it is useful to introduce the average line profile $\overline{\phi}(z)$ defined as

$$\overline{\phi}(z) = \frac{1}{(1+z)(\nu_2 - \nu_1)} \int_{\nu_1(1+z)}^{\nu_2(1+z)} \phi(\nu)\,d\nu. \tag{6}$$

Further, we also assume that the FRB is located at an angle $\boldsymbol{\theta}$ relative to the telescope's beam centre, and use $B(\boldsymbol{\theta})$ to denote the normalized beam pattern. The fluence that will be observed by this telescope is given by

$$\overline{F} = \frac{E\overline{\phi}(z)B(\boldsymbol{\theta})}{4\pi r^2}. \tag{7}$$

2.1 Pulse broadening

An electromagnetic pulse from cosmological distances gets broadened by three factors – cosmic expansion, dispersion and scattering, the later two due to propagation through the ionized interstellar medium (ISM) and the IGM. The cosmic expansion simply broadens the pulse by a factor of $(1 + z)$. The observed pulse width w for an extragalactic event with an intrinsic pulse width of w_i is given by

$$w = \sqrt{w_{\rm cos}^2 + w_{\rm DM}^2 + w_{\rm sc}^2} \qquad (8)$$

where $w_{\rm cos} = (1 + z)w_i$, $w_{\rm DM}$ and $w_{\rm sc}$ are respectively the contributions to the total pulse width from the cosmologically broadened intrinsic pulse width, the residual dispersion across a single frequency channel and scattering in the intervening medium.

The frequency-dependent refractive index of the ionized components of the ISM and IGM causes dispersion of a pulse propagating through it. This dispersion, which has a ν^{-2} dependence, spreads the observed pulse over a large time interval across the entire observational frequency bandwidth B. The signal is dedispersed by applying appropriate time delays to synchronize the pulse at all the frequency channels across the band. However, it is not possible to correct for the dispersion within a single frequency channel width $\Delta \nu_c$. This introduces a residual dispersion broadening $w_{\rm DM}$ which, under the assumption $\Delta \nu_c / \nu_0 \ll 1$, can be calculated using

$$w_{\rm DM} \approx 8.3 \times 10^6 \, \frac{{\rm DM} \, \Delta \nu_c}{\nu_0^3} \, {\rm ms} \qquad (9)$$

where ν_0 is the central frequency of the observation expressed in MHz and the DM is expressed in pc cm^{-3}. Note that the fact that we are holding the frequency in the denominator of equation (9) fixed at the value ν_0 instead varying it from channel to channel will introduce a few per cent error in the case of broad-band observations.

As mentioned earlier, the total line-of-sight DM has roughly three contributions respectively originating from the Milky Way (DM$_{\rm MW}$), the IGM (DM$_{\rm IGM}$) and the host galaxy (DM$_{\rm Host}$) of the source, and we can write

$$\rm DM = DM_{MW} + DM_{IGM} + DM_{Host} \,. \qquad (10)$$

We can estimate the electron density along different lines of sight in the Milky Way by from the NE2001 model (Cordes & Lazio [2002]) and use this to calculate DM$_{\rm MW}$ along the line of sight to the FRB. We use DM$_{\rm MW} = 60$ pc cm^{-3} as a representative value for directions away from the Galactic plane $(b > 5)$. For the host galaxy, we assume that it is similar to the Milky Way with the difference that we have no idea of the position of the FRB relative to the disc of the host galaxy and we have to allow for the possibility that the FRB signal reaches us through the disc of the host galaxy. We therefore expect that on the average the FRB signal will traverse a larger distance through the ISM of the host galaxy as compared to the distance it traverses through the Milky Way, and we use a slightly larger value DM$_{\rm Host} = 100/(1 + z)$ pc cm^{-3} for the host galaxy contribution. The $(1 + z)$ factor here arises due to the cosmological expansion. We estimate the IGM contribution using (Ioka [2003])

$$\rm DM_{IGM}(z) = \frac{3cH_0\Omega_b}{8\pi G m_P} \int_0^z \frac{(1 + z')\,dz'}{\sqrt{\Omega_m(1 + z')^3 + \Omega_\Lambda}} \qquad (11)$$

where m_P is the proton mass and the other symbols have the usual interpretation.

Multipath propagation through the ionized IGM and the ISM of both the host galaxy and the Milky Way cause scatter broadening $w_{\rm sc}$ of the pulse. We expect this to predominantly arise from the IGM due

to a geometrical effect known as the lever-arm effect (Vandenberg [1976]). The theory of scatter broadening in the ionized IGM is not well understood at present, and we consider two scattering models to calculate the pulse broadening.

(i) Scattering Model I is based on the empirical fit

$$\log w_{\rm sc} = C_0 + 0.15 \log {\rm DM_{IGM}}$$
$$+ 1.1 \, (\log {\rm DM_{IGM}})^2 - 3.9 \log \nu_0 \qquad (12)$$

with $C_0 = -6.46$ given by Bhat et al. ([2004]) for pulsars in the ISM of our Galaxy. We have used $C_0 = 3.2$ to rescale this for scattering in the IGM. This value of C_0 is based on the assumption that the reference event FRB 110220 has an intrinsic pulse width of $w_i = 1$ ms. Equation (9) predicts $w_{\rm DM} = 0.17$ ms for $z = 0.8$, and we have set the value of C_0 so that equation (12) gives $w_{\rm sc} = 5.3$ ms required to match the observed pulse width $w = 5.6$ ms (Table 1). Note that in equation (12), we use ν_0 in MHz, $w_{\rm sc}$ in ms, DM in pc cm^{-3} and log denotes $\log_{10}$.

(ii) Scattering Model II is based on the temporal smearing equation for IGM turbulence given by Macquart & Koay ([2013])

$$w_{\rm sc}(z) = \frac{k_{\rm sc}}{\nu^4 Z_L} \int_0^z D_H(z') \, {\rm d}z' \int_0^z (1 + z')^3 D_H(z') \, {\rm d}z' \qquad (13)$$

where

$$D_H(z) = (\Omega_m (1 + z)^3 + \Omega_\Lambda)^{-1/2}, \qquad (14)$$

$$Z_L = (1 + z)^2 \left[(1 + z) - \sqrt{z(1 + z)} \right]^{-1} \qquad (15)$$

and we use $k_{\rm sc} = 8.5 \times 10^{13}$ ms MHz^4 for the normalization constant. As with Scattering Model I, the value of the normalization constant is set to reproduce the observed pulse width of FRB 110220 assuming that it has an intrinsic pulse width $w_i = 1$ ms.

For both the scattering models that we have considered here, the value of the normalization constant would change if we assume a different intrinsic pulse width for FRB 110220. We have tried out $w_i = 0.5$ and 2 ms in order to assess how this would affect the results of our analysis.

Note that Scattering Model I is based on an empirical fit which is observationally well established within the ISM of our Galaxy. Given the high-DM part of the model is largely constrained by measurements of pulsars in the Galactic plane, it is effectively a representation of turbulence and clumpiness in the ISM. The nature of turbulence may be different for IGM and hence it is not clear whether the same fit can be rescaled to correctly quantify IGM scattering. In contrast, Scattering Model II is based entirely on a theoretical model for the IGM scattering. This model, however, has not been observationally verified. Given our present lack of knowledge, we have used the two different scattering models to estimate the possible impact on the pulse width.

Fig. 1 shows the total pulse width w (equation 8) corresponding to an FRB of intrinsic pulse width $w_i = 1$ ms located at a redshift z observed by the Parkes telescope for which $\nu_0 = 1382$ MHz and $\Delta \nu_c = 390$ kHz. Recollect that both the scattering models are normalized using FRB 110220 assuming $w_i = 1$ ms for this event, and therefore both the scattering models predict $w = 5.6$ ms at $z = 0.8$. We see that the residual DM $w_{\rm DM}$ makes a very insignificant contribution to w at all redshifts. Scatter broadening is not very important at low redshifts where we have $w \approx w_{\rm cos}$. The total pulse width is dominated by scatter broadening at large redshifts. For Scattering Model I the total pulse width is dominated by $w_{{\rm sc}_I}$ at $z \approx 0.5$, and
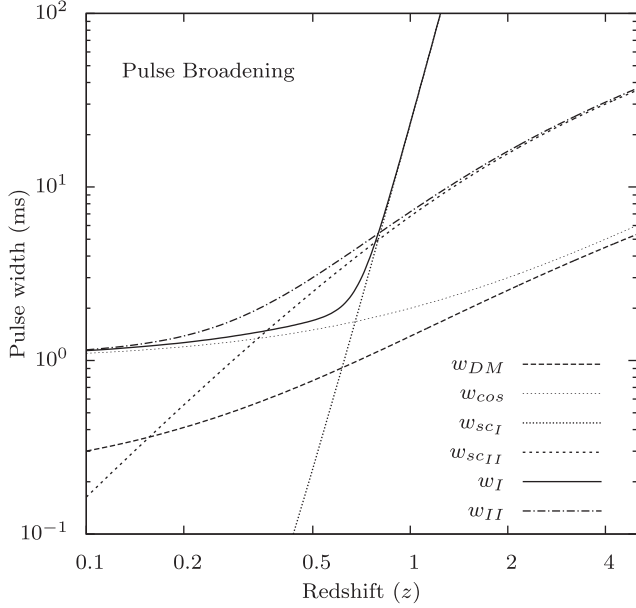
Figure 1. The predicted total pulse width assuming an FRB of intrinsic pulse width $w_i = 1$ ms located at redshift z observed by the Parkes telescope. The subscripts I and II denote the two different scattering models referred to in the text. The different components which contribute to the total pulse width are also shown individually.

w_{sc_I} increases sharply for $z \geq 0.5$. For Scattering Model II $w_{sc_{II}}$ starts making a significant contribution to w at $z \approx 0.2$, however it dominates the total w only for $z \geq 0.4$. Unlike Scattering Model I, $w_{sc_{II}}$ increases relatively gradually with z. For both the scattering models, the total pulse width is considerably in excess of w_{cos} for FRBs with $z \geq 0.5$. We have repeated the entire exercise for $w_i = 0.5$ and 2 ms, i.e. the intrinsic pulse width of the observed FRB and the normalization of the scattering model are both changed. The results, which are very similar to those shown in Fig. 1 for $w_i = 1$ ms, are not shown here. We find that the qualitative features of the total pulse width as a function of z are not very different if we change the value of w_i. Scatter broadening starts to dominate at $z \approx 0.5$, and the total pulse width is considerably larger than w_{cos} for $z \geq 0.5$.

2.2 Detection criteria and detection rate

Considering an FRB of energy E and intrinsic pulse width w_i located at redshift z, we have till now discussed how to calculate the fluence $\overline{F}$ (equation 7) and the pulse width w (equation 8) that will be observed by a given telescope. We now discuss the criteria for this particular FRB to be detected by the given telescope.

The detection criteria is decided by the telescope's system noise. The r.m.s. flux density fluctuation ΔS is given by

$$\Delta S = \frac{T_{sys}}{G \sqrt{\Delta t \, B \, N_{pol}}} \equiv \sqrt{\frac{1 \, \text{m}s}{w}} \times [\Delta S]_{1ms} \quad (16)$$

where G is the antenna gain of the primary beam, T_{sys} is the telescope's system temperature, N_{pol} is the number of polarizations the telescope detects and Δt is the integration time. We assume an integration time equal to the observed pulse width w. Since the observed FRB pulse widths are of the order of a few milliseconds, it is then convenient to express ΔS (equation 16) in terms of w and $[\Delta S]_{1ms}$ which is the r.m.s. noise for $\Delta t = 1$ ms.

An FRB with average observed flux density $\overline{S} = \overline{F}/w$ will result in a detection if

$$\frac{\overline{S}}{\Delta S} = \frac{\overline{F}}{w \, \Delta S} \geq n \,, \quad (17)$$

where n is the minimum signal-to-noise ratio required for a detection. The same criteria can be expressed in terms of a limiting fluence $F_l = n \times (1 \, \text{ms}) \times [\Delta S]_{1ms}$ as

$$\overline{F} \times \sqrt{\frac{1 \, \text{m}s}{w}} \geq F_l \quad (18)$$

Thornton et al. (2013) have only considered events with a signal-to-noise ratio greater than nine as a detection, following these authors we have used $n = 9$ for the Parkes telescope.

The detection criteria (equation 17) combined with (equation 7) implies a minimum energy

$$E_{min} = \frac{4\pi r^2 F_l}{\overline{\phi}(z) B(\boldsymbol{\theta})} \sqrt{\frac{w}{1 \, \text{m}s}} \quad (19)$$

for a telescope to detect an FRB at a redshift z and a sky position ($\boldsymbol{\theta}$) relative to the telescope's beam centre. A telescope's primary beam pattern $B(\boldsymbol{\theta})$, the antenna gain G of the primary beam and system temperature T_{sys} will, in general, vary as the telescope is pointed to different parts of the sky. To simplify the analysis, we have assumed these telescope parameters to be constant.

The number of FRB events at redshift z per unit time (in the source frame) per unit comoving volume with energy in the range E to $E + \text{d}E$ and intrinsic pulse width in the range w_i and $w_i + \text{d}w_i$ can be expressed as

$$\text{d}N = n(E, w_i, z) \, \text{d}E \, \text{d}w_i. \quad (20)$$

where $n(E, w_i, z)$ is the comoving number density of the FRB occurrence rate.

For an observation time T with a given telescope, the number of events detected (N_{det}) is expected to be

$$N_{det}(T) = T \int \text{d}z \frac{\text{d}r}{\text{d}z} \left(\frac{r^2}{1+z} \right)$$
$$\times \int \text{d}\Omega \int \text{d}w_i \int_{E_{min}(z)}^{\infty} \text{d}E \, n(E, w_i, z). \quad (21)$$

We use equation (21) to predict the FRB detection rate for any given telescope. Here it is assumed that the telescope has a sampling time ≤ 1 ms so as to be able to resolve the FRB. The factor of $(1 + z)$ in the denominator arises from the fact that a time interval of T in the observer's frame corresponds to a time interval of $T/(1 + z)$ in the source frame. The quantity within the square brackets gives the redshift distribution of the detected events. We may interpret the latter as the detection rate with the FRB source originating in the redshift interval z to $z + \text{d}z$.

3 MODELLING THE FRB POPULATION

The basic formalism introduced in the previous section requires the FRB emission line profile $\phi(\nu)$ and the comoving number density of the FRB occurrence rate $n(E, w_i, z)$ as inputs in order to predict the FRB detection rate for any given telescope. With only 16 FRB events detected to date, we do not as yet have any established models and for our work we assume very simple models for these two quantities. We discuss these models below.

The spectrum of the FRB emission is very poorly constrained at present, the detection so far being all (except FRB 110523) in the
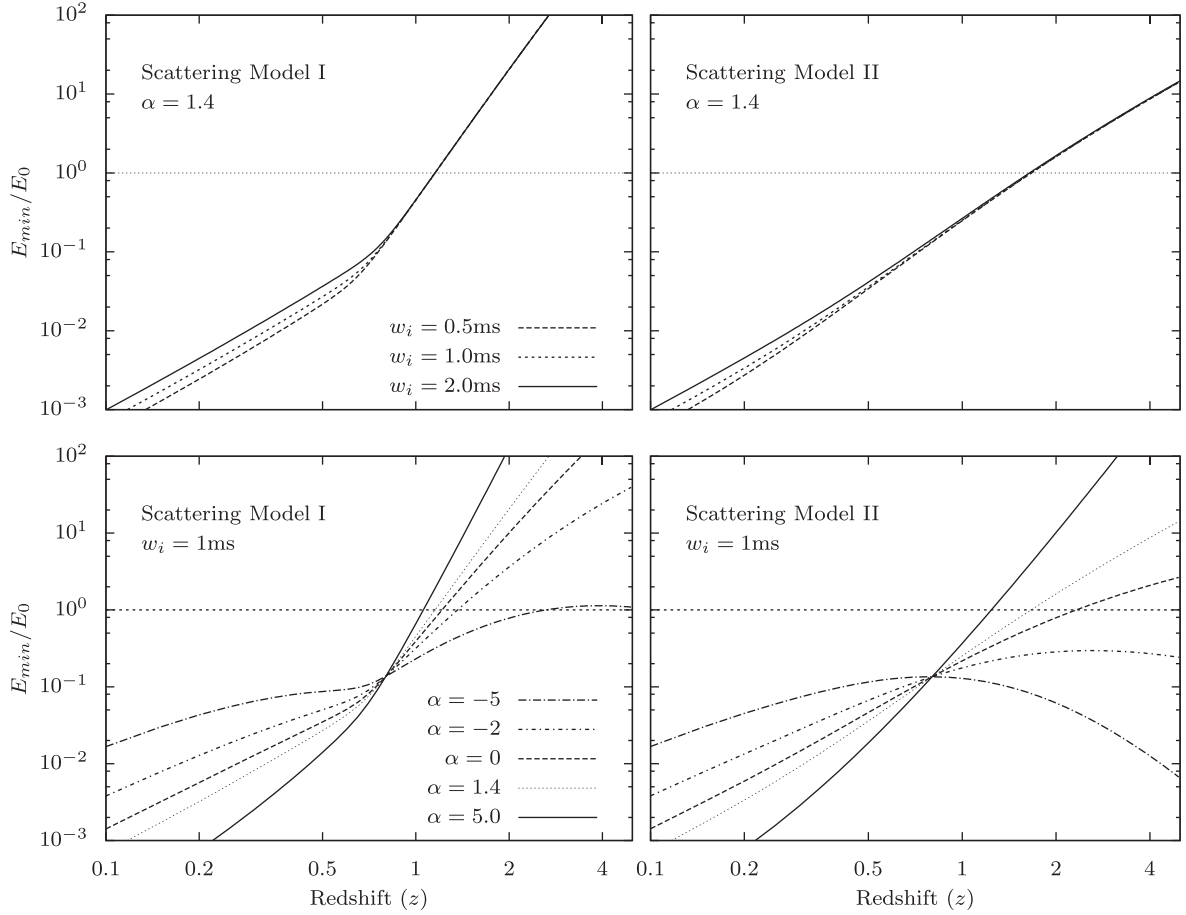
Figure 2. The minimum energy E_{min} for an FRB at redshift z to be detected at the Parkes telescope assuming that the source is located at the beam centre. The left- and right-hand panels are for Scattering Models I and II, respectively. The upper panels consider different values of the intrinsic pulse widths w_i with spectral index $\alpha = 1.4$ fixed, while the lower panels consider different values of α with $w_i = 1$ ms fixed.

L-band. The high observed flux suggests that the emission mechanism is coherent for which we expect a negative spectral index. Here we have assumed a simple power-law spectrum $S_\nu \propto \nu^{-\alpha}$ with a spectral index $-\alpha$ vary from -5 to $+5$ for which we have the normalized (equation 2) emission profile

$$\phi(\nu) = \left[\frac{1-\alpha}{\nu_b^{1-\alpha} - \nu_a^{1-\alpha}} \right] \nu^{-\alpha} \quad (22)$$

and the average line profile has the form

$$\overline{\phi}(z) = K(\alpha)(1+z)^{-\alpha} \quad (23)$$

where $K(\alpha)$ is

$$K(\alpha) = \frac{1}{\nu_2 - \nu_1} \left[\frac{\nu_2^{1-\alpha} - \nu_1^{1-\alpha}}{\nu_b^{1-\alpha} - \nu_a^{1-\alpha}} \right]. \quad (24)$$

Although non-detection in searches at different wavelengths give constraints on the spectral index, we consider the range $-5 \leq \alpha \leq 5$ for completeness.

The minimum energy E_{min} (equation 19) can now be expressed as

$$E_{min} = \frac{4\pi r^2 F_l}{B(\theta)} \left[\frac{(1+z)^\alpha}{K(\alpha)} \right] \sqrt{\frac{w}{1 \text{ ms}}}. \quad (25)$$

Fig. 2 shows E_{min} as a function of z assuming the FRB to be located at the centre of one of the beams of the Parkes telescope ($B(\theta) = 1$). We expect the FRBs to typically have an energy E

$\sim E_0$, and we have shown E_{min} in units of the reference energy E_0. The upper panels show the results for three different values of the intrinsic pulse width w_i with $\alpha = 1.4$ fixed, while the bottom panels shows the results for three different values of α with $w_i = 1$ ms fixed. We do not find a very big difference if the value of w_i is changed; however, the results vary considerably if the value of α is changed. We first discuss only the positive values of α (≥ 0). For Scattering Model I, we find that the value of E_{min} increases sharply for $z \geq 1$ due to the steep increase in the pulse width (Fig. 1). The value of E_{min} increases more gradually in Scattering Model II. In all cases the main feature is that E_{min} increases with redshift and exceeds E_0 in the range $1 \leq z \leq 2$. Assuming that the FRBs have energy $E \sim E_0$, this imposes a cut-off redshift z_c such that observation with the Parkes telescope are only sensitive to FRBs with $z \leq z_c$. We see that the value of z_c is largely insensitive to w_I, however it shifts to smaller z if α is increased from 0 to 5. In all cases we find $1 \leq z_c \leq 2$ for the Parkes telescope. For $\alpha \geq 0$, our models predict that we do not expect the Parkes telescope to detect FRBs with $z > 2$, consistent with the observations summarized in Table 1. Next, considering the negative values of α we find that the results are quite different from those for $\alpha \geq 0$. The difference is particularly pronounced for Scattering Model II where we see that the value of E_{min} decreases with z for $\alpha = -5$. In this case we do not have a cut-off redshift and we expect the Parkes telescope to detect FRBs out to arbitrarily high redshifts, a prediction that is inconsistent with the observations summarized in Table 1. A similar

problem also arises for $\alpha = -2$, however it is not as severe as for $\alpha = -5$. Based on these findings, we have restricted the subsequent analysis to α values in the range $-2 \leq \alpha \leq 5$.

We now shift our attention to the comoving number density of the FRB occurrence rate $n(E, w_i, z)$. Since the cut-off redshift z_c for FRB detection, at least for the Parkes telescope, does not depend on the intrinsic pulse width w_i (Fig. 2) we assume that all the FRBs have the same intrinsic pulse width of $w_i = 1$ ms. Further, since we expect all the detected FRBs to be within $z \leq 2$, as assume that $n(E, w_i, z)$ is constant over the limited redshift range of our interest. The function $n(E, w_i, z)$ is now just a function of E, and we have considered two simple models for the E dependence.

(i) The delta-function model where all the FRBs emit the same energy E_0 and

$$n(E, w_i, z) = n_0 \, \delta(E - E_0). \tag{26}$$

(ii) The Schechter luminosity function model where the FRB energies have a spread, the energy distribution being given by the Schechter function

$$n(E, w_i, z) = \frac{n_0}{E_0} \left(\frac{E}{E_0} \right)^\gamma \exp\left(-\frac{E}{E_0} \right). \tag{27}$$

We consider both positive and negative values of the exponent γ. The negative values of γ require a lower cut-off to make the distribution normalizable. We have considered a cut-off energy of $E_0/100$ for our analysis.

We have used the FRBs observed by the Parkes telescope to determine the value of the normalization constant n_0 which is a free parameter in both the models for $n(E, w_i, z)$. Though there are fourteen FRBs detected at the Parkes telescope, it is not possible to use all of them to calculate an event rate because the exact duration of the observation is not known. The four FRBs detected by Thornton et al. (2013) correspond to an effective observation time of 298 d with a single beam of the Parkes telescope, and we have used the inferred detection rate along with equation (21) to determine the value of n_0. Note that Champion et al. (2015) have estimated a slightly lower FRB occurance rate than Thornton et al. (2013) but they are consistent with each other within 1σ uncertainies.

As noted earlier, the FRB distribution predicted for Parkes extends to arbitrarily large redshifts for negative values of α. We see this in the topmost right-hand panel of Fig. 3 ($\alpha = -2$ and Scattering Model II) where the FRB predictions do not fall of even at $z > 4$. This is even more severe for $\alpha = -5$ which has not been shown here. This poses a problem for the z integral in equation (21), and it is necessary to assume an upper limit to obtain a finite prediction. We have assumed an upper limit of $z = 5$ for calculating n_0. While the upper limit $z = 5$ has been introduced here for mathematical convenience, we may interpret this as the redshift beyond which the FRB population ends abruptly. Finally, we note that the non-detection of any FRBs in the search by Rane et al. (2016) seem to indicate that the FRB rate is possibly a factor of 3–5 times smaller than that inferred from these four Parkes FRBs.

Redshift estimates are available for all the 14 FRBs detected by the Parkes telescope (Table 1). The redshift distribution of the detected FRBs provides an independent constraint on any model for the FRB population. We now compute the redshift distribution predicted by our models (equation 21) and compare these with the observed redshift distribution of the 14 Parkes FRBs. 6 of the 14 Parkes FRBs are in the redshift range $0.4 \leq z \leq 0.6$. We see that most of the models also predict redshift distributions which peak around the same z range. Considering first the delta-function model

where all the FRBs have the same energy E_0, we see that the redshift distribution extends out to larger redshifts in Scattering Model II as compared to Scattering Model I. The redshift distribution also extends out to larger redshifts if the value of α is decreased. Both of these effects can be understood in terms of the cut-off redshift z_c introduced while discussing Fig. 2. The Schechter luminosity function introduces a spread in the FRB energies. The relative abundance of low-energy FRBs increases if the value of γ is reduced, and we see that the entire redshift distribution shifts to lower redshifts for negative values of γ.

We see that most of the models considered here are roughly consistent with the redshift distribution of the observed FRBs (Fig. 3). As mentioned earlier, the predicted FRB distribution extends beyond $z = 4$ for $\alpha = -2$ and Scattering Model II whereas the observed redshift distribution falls off well within $z = 1.5$. Unfortunately, the number of FRBs which have been detected to date is too small to place meaningful constraints on the models which we have considered. However, we anticipate that larger numbers of FRBs will be detected in future and it will be possible to constrain both the scattering models as well as the models for the FRB population using the redshift distribution of the detected events.

4 PREDICTIONS FOR OWFA

We now use the formalism and the various models presented in the earlier parts of this paper to study the prospects of detecting FRBs with the ORT LS and the two different phases of OFWA (PI and PII). In Phase I, the signal from $N_d = 24$ successive dipoles are combined to form an individual antenna, and there are a total of $N_A = 40$ such antennas. We have $N_d = 4$ and $N_A = 264$ for Phase II. The aperture dimensions and other details are tabulated in Table 2.

Each phase of OWFA has N_A antennas which can be operated together as a linear radio-interferometric array. However, for the present analysis we consider a simpler situation where the signals from the N_A antennas are incoherently added. A more detailed analysis using the full beam forming capability of OWFA will be presented in a later paper. Consequently, the FoV is the same as that of a single antenna (given in Table 2) but the r.m.s. flux density fluctuation is reduced to $[\Delta S]_{1ms}/\sqrt{N_A}$. The ORT LS and OWFA PI and PII all have anisotropic beam patterns which we have parametrized as

$$B(\boldsymbol{\theta}) = \mathrm{sinc}^2 \left(\frac{\pi d \theta_x}{\lambda} \right) \mathrm{sinc}^2 \left(\frac{\pi b \theta_y}{\lambda} \right) \tag{28}$$

(Ali & Bharadwaj 2014) where we have the antenna aperture $b \times d$ (Table 2) and λ is the observing wavelength. Here, we have used the flat-sky approximation, and (θ_x, θ_y) are the components of the vector $\boldsymbol{\theta}$ on the plane of the sky. We note that the flat sky approximation does not hold for Phase II which has a very large FoV; however, this is justified by the fact that the error introduced by this assumption is small compared to the other uncertainties in our modelling of the scattering and the FRB population.

Our predictions for the FRB detection rate are shown in Fig. 4. We have taken minimum signal-to-noise ratio $n = 10$ for these predictions. We see that the predicted detection rate is highest for PII which has the largest FoV and the largest frequency bandwidth. We expect to detect somewhere between ~ 0.01 to 1000 FRBs d^{-1} with PII, depending on the spectral index of the FRB emission. We have a higher detection rate for larger positive values of α, the detection rates are also higher for Scattering Model I as compared to Model II. The predicted detection rates fall by roughly an order of magnitude for PI, and roughly two orders of magnitude for LS
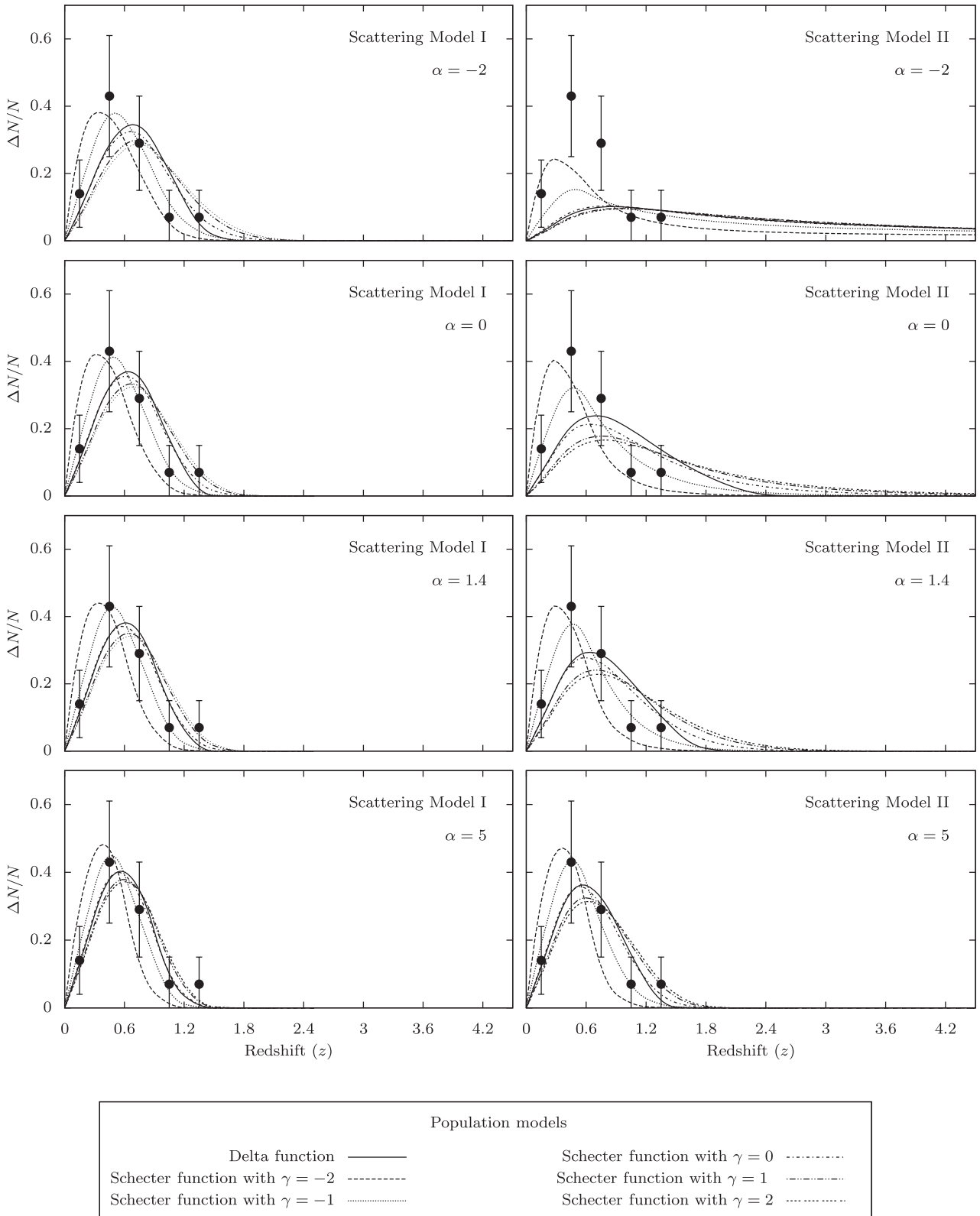
Figure 3. The data points show the redshift distribution $\Delta N/N$ of the 14 FRBs detected at the Parkes telescope, the data has been binned with $\Delta z = 0.3$, ΔN is the number of FRBs in each bin and N is the total number of FRBs. The error bars show the $1 - \sigma$ Poisson errors for the data. The theoretical predictions for the different models are shown as continuous curves. These curves show $N^{-1} (dN/dz)$ normalized so that the total area is same for all. Unfortunately, the number of FRBs which have been detected to date is too small to place meaningful constraints on the models which we have considered.
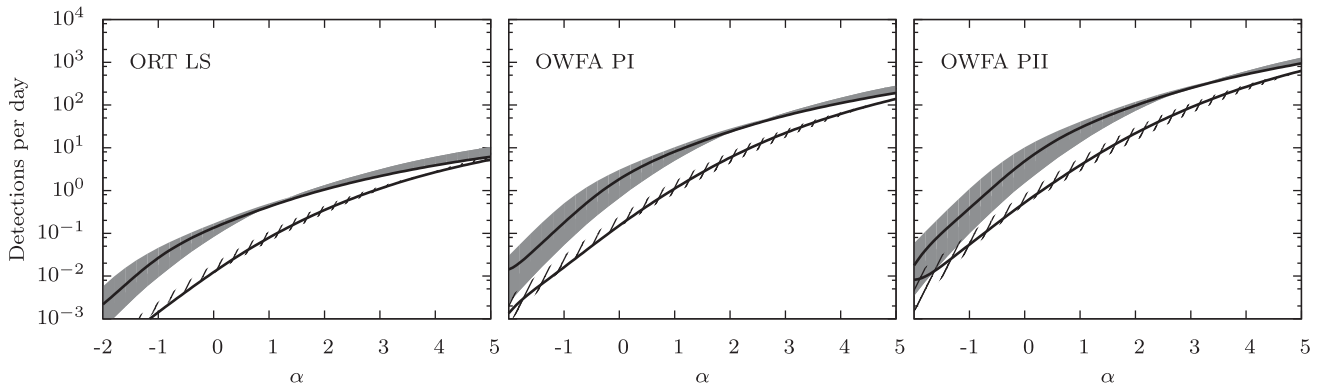
Figure 4. The expected FRB detection rates as a function of α for ORT LS, and OWFA PI and PII assuming 1024 frequency channels spanning the bandwidth B given in Table 2. The grey shaded and hatched regions correspond to Scattering Model I and II, respectively, the solid curves passing through these regions show predictions for the delta-function FRB population model while the boundaries of the regions enclose the curves corresponding to all the other models considered in Fig. 3.

as compared to PII. Considering $\alpha = 1.4$ which has been proposed to be the most likely value for the coherent FRB emission (Lorimer et al. 2013), we expect to detect ~10 to ~100 FRBs per day with PII. This is quite encouraging even if we take into account the fact that Rane et al. (2016) have suggested that the FRB occurrence rates estimated from the FRBs detected by Thornton et al. (2013) may be a factor of 3–5 larger than the actual FRB occurrence rate.

5 SUMMARY AND CONCLUSION

The source of the FRBs is still largely unknown. Assuming the FRBs to be of extragalactic origin, we have developed a formalism to predict the FRB detection rate (equation 21) and the redshift distribution of the detected events for a telescope with given parameters. We have adopted FRB 110220 (Table 1) as the reference event for our entire analysis. None of the FRBs detected to date have a direct redshift measurement, and the redshifts of all the detected FRBs (Table 1) have been inferred from the observed DMs. The value of the inferred redshift depends on the Milky Way and host galaxy DM contribution assumed in the analysis, and different authors have assumed different values. For our analysis we have adopted the inferred z values from the references listed in Table 1. In contrast, the redshift z in our analytic calculations and in Figs 1–3 refer to the actual cosmological redshift of the FRB which is unaffected by our assumptions for DM_{MW} and DM_{Host}. The assumed values only affect the observed pulse width w through equations (8)–(10). Further, the DM makes a subdominant contribution to the total pulse width w for the entire range considered here (Fig. 1), and consequently our predictions are largely unaffected by DM_{MW} and DM_{Host}.

The FRB pulse width plays an important role in determining the detection rates. At present we lack adequate understanding of pulse broadening due to scattering in the ionized IGM, and we consider two different alternatives to model this. Scattering Model I is based on an observational fit given by Bhat et al. (2004) for pulsars in the ISM of our Galaxy, we have extrapolated this for FRB pulse broadening in the IGM. In contrast, Scattering Model II is based on a theoretical calculation given by Macquart & Koay (2013), and it has no observational confirmation at present. Both the scattering models are normalized to reproduce the observed pulse width of FRB 110220, assuming that it has an intrinsic pulse width of $w_i = 1$ ms. For the Parkes telescope, we find that in both the models scatter broadening starts to dominate the total pulse width at $z \approx$

0.5 (Fig. 1). In Model I, the total pulse width increases steeply for $z > 0.5$ whereas a more gradual increases is predicted by Model II. We also find that the $z > 0.5$ behaviour is not significantly modified if we assume an intrinsic pulse width of $w_i = 0.5$ or 2 ms for FRB 110220. The cosmological broadening of the intrinsic pulse width dominates at lower z.

The total energy in the FRB pulse and its spectrum also play an important role in determining the FRB detection rate. We have introduced the FRB energy E and the FRB emission profile $\phi(\nu)$ (equation 1) to model the FRB energy spectrum. For our work we have assumed a power law $\phi(\nu) \propto \nu^{-\alpha}$ (equation 22) where α is the (negative) spectral index. In this paper we have presented results for α values in the range $-5 \leq \alpha \leq 5$, however most of the analysis is restricted to $\alpha \geq -2$.

It is necessary to model the FRB population in order to make predictions for the detection rate. We have quantified the FRB population through $n(E, w_i, z)$ which gives the comoving number density of the FRB occurrence rate. For our work we have assumed that $n(E, w_i, z)$ does not vary with z over the limited redshift range of our interest. Further, all the FRBs are assumed to have the same intrinsic pulse width $w_i = 1$ ms. For the E dependence we have adopted the simplest delta-function model where all the FRBs have the same energy $E_0 = 5.4 \times 10^{33}$ J which is the estimated energy for FRB 110220. We have also considered a set of models where the E values have a spread around E_0. In this case the E distribution has the form of a Schecter luminosity function (equation 27). We present results for both negative and positive values of γ. The models are all normalized to reproduce the event rate corresponding to the four FRBs detected at Parkes by Thornton et al. (2013).

We have calculated the FRB redshift distribution predicted by our models for observations with the Parkes telescope. The predictions indicate that we do not expect to detect FRBs with redshifts $z > 2$ with the Parkes telescope (Fig. 2). The redshift distribution (Fig. 3) peaks in the range $0.4 \leq z \leq 0.6$ for most of the models which we have considered. We find that most of the models that we have considered are consistent with the redshift distribution of the 14 FRBs observed by the Parkes telescope. However, some of the models with $\alpha \leq -2$ predict a redshift distribution that extends beyond $z \geq 4$ while the observed FRB distribution is restricted within $z \leq 1.5$. The number of FRBs observed to date is too small to conclusively constrain the models which we have considered here. Our prediction however indicate that it will be possible to distinguish

between the different models when more FRB data becomes available in future.

Finally, we have used the formalism and the different models presented here to predict the FRB detection rate expected at the ORT LS and the OWFA PI and PII. The main point to note here is that OWFA PII has a FoV which is 880 times larger than the individual beam of the Parkes telescope where most of the FRBs have been detected. Further, the existing FRBs have all been detected in the *L*-band ($\sim$1–2 GHz) whereas ORT and OWFA operate around 326.5 MHz. We predict that we expect to detect somewhere between $\sim$0.01 to 1000 FRBs d^{-1} with PII, depending on the value of α. The upcoming OWFA PII holds the potential of dramatically increasing the population of detected FRBs, thereby opening a new window to unravel the source of these mysterious events. We plan to present a detailed treatment of the predictions for ORT and OWFA in a subsequent work.

REFERENCES

Ali S. S., Bharadwaj S., 2014, J. Astrophys. Astron., 35, 157
Bannister K. W., Madsen G. J., 2014, MNRAS, 440, 353
Bhat N. D. R., Cordes J. M., Camilo F., Nice D. J., Lorimer D. R., 2004, ApJ, 605, 759
Burke-Spolaor S., Bannister K. W., 2014, ApJ, 792, 19
Champion D. J. et al., 2015, preprint (arXiv: 1511.07746)
Coenen T. et al., 2014, A&A, 570, A60
Cordes J. M., Lazio T. J. W., 2002, preprint (astro-ph/0207156)
Falcke H., Rezzolla L., 2014, A&A, 562, A137
Ioka K., 2003, ApJ, 598, L79
Karastergiou A. et al., 2015, MNRAS, 452, 1254
Kashiyama K., Ioka K., Mészáros P., 2013, ApJ, 776, L39
Keane E. F., Petroff E., 2015, MNRAS, 447, 2852
Keane E. F., Stappers B. W., Kramer M., Lyne A. G., 2012, MNRAS, 425, L71
Loeb A., Shvartzvald Y., Maoz D., 2014, MNRAS, 439, L46
Lorimer D. R., Bailes M., McLaughlin M. A., Narkevic D. J., Crawford F., 2007, Science, 318, 777
Lorimer D. R. et al., 2013, MNRAS
Macquart, J. P., Koay, J. Y., 2013, ApJ, 776, 125
Masui K. et al., 2015, Nature, 528, 523
Mottez F., Zarka P., 2014, A&A, 569, A86
Petroff E. et al., 2015, MNRAS, 447, 246
Prasad P., Subrahmanya C. R., 2011a, preprint (arXiv:1102.0148)
Prasad P., Subrahmanya C. R., 2011b, Exp. Astron., 31, 1
Rane A. et al., 2016, MNRAS, 455, 2207
Ravi V., Shannon R. M., Jameson A., 2015, ApJ, 799, L5
Spergel D. N. et al., 2003, ApJS, 148, 175
Spitler L. G. et al., 2014, ApJ, 790, 101
Thornton D. et al., 2013, Science, 341, 53
Totani T., 2013, PASJ 65, L12
Vandenberg N. R., 1976, ApJ, 209, 578

This paper has been typeset from a TeX/LaTeX file prepared by the author.